Comparison of the Diffusive Flame Structure for Dodecane and OME_X Fuels for Conditions of Spray A of the ECN

José V. Pastor, José M. García-Oliver, Carlos Micó, Francisco J. Tejada
CMT-Motores Térmicos. Universitat Politècnica de València

Abstract

A comparison of the flame structure for two different fuels, dodecane and oxymethylene dimethyl ether (OME_X), has been performed under condition of Spray A of the Engine Combustion Network (ECN). The experiments were carried out in a constant pressure vessel with wide optical access, at high pressure and temperature and controlled oxygen concentration. The flame structure analysis has been performed by measuring the formaldehyde and OH radical distributions using planar Laser-Induced Fluorescence (PLIF) techniques. To complement the analysis, this information was combined with that obtained with high-speed imaging of OH^* chemiluminescence radiation in the UV. Formaldehyde molecules are excited with the 355-nm radiation from the third harmonic of a Nd:YAG laser, whilst OH is excited with a wavelength of 281.00-nm from a dye laser. In both cases, the beam was transformed into a laser sheet in order to excite an axial flame plane and the fluorescence radiation was collected with an intensified camera (ICCD) and proper filtering. Consequently, two-dimensional maps in the axial flame plane were obtained at different instants after the start of injection (ASOI). Signal from both formaldehyde and OH chemical species can be compared, in order to analyze spatial distribution and interaction. When dodecane and OME_X are compared, several differences arise. The second one presents larger lift-off length but remarkably shorter flame length. Additionally, it has been possible to appreciate for this fuel a lower amount of soot formation during combustion.

Introduction

Pollutant emissions control in the automotive industry is increasingly restrictive, which is pushing the development of several emerging technologies in the last few years. Current advanced aftertreatment systems are effective in reducing engine out emissions in Compression Ignition engines, but its complexity and cost increases accordingly [1]. Consequently, technologies oriented towards direct reductions of in-cylinder emissions are gaining interest. In this regard, the advanced combustion modes such as low temperature combustion (LTC) are considered as promising ways to reduce NO_X and soot emissions whilst keeping high combustion efficiency [2, 3], which could contribute to the simplification of the aftertreatment devices. The use of high exhaust gas recirculation rates (EGR) combined with more premixed conditions than in conventional diesel combustion allow achieving extremely low soot and NO_X emissions [4]. Even potentially better emission reductions can be obtained with other strategies such as dual fuel dual mode combustion or Reactivity controlled compression ignition (RCCI) in compression ignition engines in the whole combustion map operating range as recently shown in [5].

Besides the need of fuels well adapted to these combustion modes, it is necessary to minimize the harmful greenhouse gas (GHG) emissions produced by the transportation sector [6]. Advanced fuels from renewable sources become an option to achieve the targets imposed by legislation [7, 8]. Among the many different fuel types nowadays available which produce fair results under different engine situations [9, 10, 11, 12], the family of oxymethylene dimethyl ethers (OME_X) has gained interest in recent years because of its potential to reduce engine out emissions whilst maintaining engine performance [5, 13, 14]. In addition, OME_X fuels can be produced with renewable electricity, becoming one of the most interesting synthetic fuels (e-fuels) for future transportation [7, 8]. The OME_X fuels are blends of molecules with CH_3-O-(CH_2-O)$_X$-CH_3 chemical structure being with x in the range of 1–6 [15]. The shortest chain OME_1 presents storage and handling problems due to the very low boiling point, but chemical structures of OME_X with longer chains (x = 3,4,5,6) are considered more interesting as they contain properties more similar to fossil diesel [16]. In any case, due to the lack of C-C bonds and the high number of oxygen atoms in the molecule, the OME_X combustion process is practically soot free, which makes it an interesting alternative fuel to replace diesel or to be blended with it completely, or partially by blending in OME_X [17].

Some studies on OME_X fuels are available in literature showing good results for soot reduction in either optical vessels [15], optical engines [18], single cylinder diesel engines [17] or multicylinder engines [13]. However, to the authors knowledge, there are no studies analyzing the details of the flame structure of OME_X sprays, and the study of different physicochemical phenomena that occur during the fuel combustion process is a key factor for a better understanding its behavior in the engine. In order to ensure reliability of the results of the current study about the flame structure, normalized experimental conditions have been considered. In this sense, operating conditions based on Spray A of the Engine Combustion Network (ECN) have been selected since a large number of experimental results for dodecane sprays under these conditions and with a vast number of experimental techniques are available to the scientific community [19].

Experimental methodology

High-pressure high-temperature vessel

The study of effects of combustion on spray dynamics of a single injection under quiescent conditions were performed in a high-pressure and high-temperature test chamber, in which the thermodynamic conditions similar to a diesel engine can be obtained. The vessel is classified as a constant-pressure flow (CPF) facility, as the operating conditions are reached by a continuous high-pressure high-temperature flow, up to 15 MPa and 1100 K within the chamber. The vessel is equipped with three quartz windows providing optical access to the test area [20]. The vessel has a frontal window with a diameter of 180 mm of diameter, and two 125-mm lateral windows with respect the position of the injector to image the sprays from the side (see Figure

1) [21]. In this work, air was diluted with nitrogen, so that oxygen concentration was reduced to 15%.

A summary of the main parameters of the facility is shown in Table 1.

Table 1. Characteristics of the high-pressure high-temperature vessel.

Facility type	CPF
Chamber diameter	200 mm
Chamber height	244 mm
Frontal window diameter	180 mm
Lateral window diameter	125 mm
Max. pressure	15 MPa
Max. temperature	1100 K
Max. density (at 900 K)	53 kg/m^3
Main heather power	30 kW
Flow rate	20 to 70 Nm^3/h

A conventional common-rail together with a solenoid-activated single-hole nozzle were used in this work. The nozzle geometry corresponds to Spray A from the ECN, with a conical orifice (K = 1.5) and 90 µm outlet diameter. Besides, a diaphragm pump using polymerizing tetrafluoroethylene was employed, which is more appropriate for low-lubricant hydrocarbons than conventional fuel pumps. The system reaches up to 230 MPa injection pressure.

The operating conditions chosen for this work are based on Spray A specifications. They are summarized in Table 2.

Table 2. Summary of the Spray A conditions with parametric variations.

Gas temperature	900 K
Gas density	22.8 kg/m^3
Oxygen (vol)	15%
Injection pressure	150 MPa

Fuels

In this work, both dodecane and OME$_X$ were studied. The first, the molecular formula is $C_{12}H_{26}$ with purity ≥ 99%. The oxymethylene dimethyl ethers (OME$_X$) are synthetic fuels (e – fuels), formed by the chemical structure $CH_3 – O – (CH_2 – O)_x – CH_3$, with being x in the range of 1-6. In our case, the OME$_X$ fuel used is a blend containing 0.01% of OME$_1$, <0.01% of OME$_2$, 57.90% of OME$_3$, 28.87% of OME$_4$, 10.07% of OME$_5$ and 1.91% of OME6. Some physicochemical properties of interest are presented in Table 3.

Table 3. Dodecane and OME$_X$ properties.

Fuel	**Dodecane**	**OME$_X$**
Density [kg/m^3] (15 °C)	751.2	1057.1
Viscosity [mm^2/s] (40 °C)	1.439	1.082
Cetane number [-]	74	68.6
Initial boiling point (ºC)	214	144.9
Lubricity [µm]	563	320
Flash point [ºC]	83	65
Lower heating value [MJ/kg]	44.2	19.21
Carbon content [% m/m]	84	44.2
Oxygen content [% m/m]	0	45

Optical techniques

Both fuels were characterized by means of optical techniques. OH* chemiluminescence as well as OH and formaldehyde PLIF were applied for this purpose. A diagram of the optical set up is shown in Figure 1.

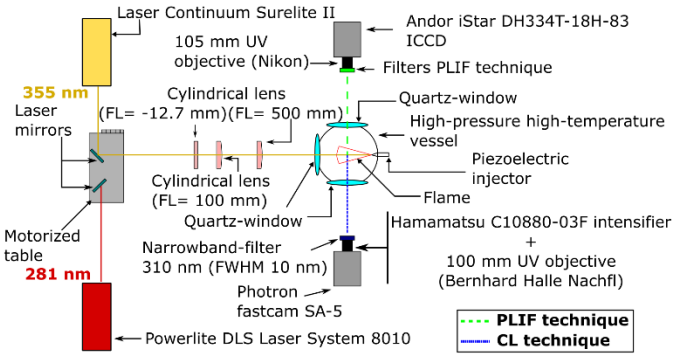

Figure 1. Experimental setup for PLIF (formaldehyde and OH) and CL (OH*) techniques.

OH chemiluminescence imaging*

Chemiluminescence is defined as the emission of electromagnetic radiation produced by a chemical reaction. The emission intensity is a function of the concentration of the chemical species involved in the reaction. As chemiluminescence is a spontaneous radiation, it is possible to employ a rather simplified optical set up, as any external light source is required. In this work, the radiation emitted by the excited-state hydroxyl radical (OH*) has been recorded, as it is considered an excellent indicator of the regions were high-temperature reactions under near stoichiometric conditions take place. These areas correspond to the flame front, and allow defining characteristic parameters of the combustion reaction such as the lift-off length (LOL) [22].

For this purpose, high-speed OH* chemiluminescence was recorded at 25 kHz with an exposure time of 39.75 µs. A high-speed CMOS camera (Photron fastcam SA-5) was used, lens-coupled to a high-speed intensifier (Hamamatsu C10880-03F) with a 1:1 relay optics. The photocathode of the intensifier is a multialkali (S-20), which allows detection from UV to near IR (spectral response: 185-900 nm). Light was collected by a 100-mm UV objective (OUC 25.50 by Bernhard Halle Nachfl, f/4) and a narrowband filter centered near the OH* peak emission, at 310 nm (10 nm FWHM). The resolution was 5.43 pixel per mm.

Intensifier settings were adjusted between the fuels to utilize the full dynamic range of the camera, while preventing overexposure. For dodecane, the gain of the intensifier was se to 75%, while for OME$_X$ it was set to 80%. The gating of the intensifier was the same as the

exposure time of the high-speed camera. The experimental setup is presented in Figure 1.

For each fuel, 21 complete combustion events were recorded without PLIF laser emissions, to avoid any damage of the intensifier due to the high intensity of the PLIF signal in comparison to the OH* chemiluminescence. Besides, it ensured no crosstalk between both radiation sources. The images obtained with the OH* chemiluminescence setup are per default line-of-sight integrated.

PLIF imaging

Laser Induced Fluorescence (LIF) techniques are based on fluorescent properties of molecules. When these molecules absorb electromagnetic energy at a certain frequency, acquire a higher energy state (excitation) and then return to the initial one. They may do so by releasing this energy (spontaneous emission) in form of electromagnetic radiation (fluorescence). The spectral characteristics of the radiation are conditioned by the molecule's characteristics [24].

Planar Laser-Induced Fluorescence (PLIF) technique used in this work is based on inducing the fluorescence of formaldehyde and OH radicals, with a short-duration laser pulse (7ns). The circular beam is transformed into a sheet in order to obtain a planar fluorescence of the species. This allows obtaining two-dimensional maps of the spatial distribution of the molecules that are excited by the laser radiation, at a certain plane within the flame. On one hand, formaldehyde characterizes low temperature reactions, which may be occurring during the ignition delay period or in some particular zones of developed Diesel flames [25, 26]. On the other hand, the OH radicals provide information off the high-temperature reaction zones that appears during the pre-mixed phase of diesel combustion and the second stage ignition of diesel combustion [27]. Besides, the appearance of these radicals indicates the start of ignition of the fuel.

PLIF was performed on formaldehyde molecules in the $\widetilde{A}^1A_2 - \widetilde{X}^1A_1$ system [28]. To excite this species a Nd:YAG laser (Laser Continuum Surelite II) was used, working with the third harmonic at 355 nm [29]. The energy output at this wavelength was 45 mJ/pulse at a lasing frequency of 10 Hz. A long-pass filter cutting at 400 nm (Newport 20CGA-400) and a band-pass filter centered at 390 nm (125 nm FWHM) were combined to isolate the fluorescence radiation of the formaldehyde molecules. The transmittance spectrum is presented in Figure 2.

PLIF of OH radicals was performed in the $A^2\Sigma^+ - X^2\Pi$ system. To excite the OH radical molecules, a laser beam at 281.00 nm is used. To generate this radiation, the second harmonic of a Nd:YAG laser (Powerlite DLS Laser System 8010) was used to pump a dye laser (Vista Dye Laser) with Rhodamine 590. The radiation was tuned to 562.00 nm and the output frequency was doubled (Vista FX Frequency Extension) to obtain 281.00 nm. The energy output at this wavelength was 35 mJ/pulse and the lasing rate was 10 Hz. A narrowband filter centered at 310 nm (10 nm FWHM) was used to isolate the fluorescence signal. Its transmittance spectrum can be observed in Figure 3. In this case, the filter is not narrow enough to completely remove the laser radiation. For this reason, certain scattering signal was registered together with the fluorescence.

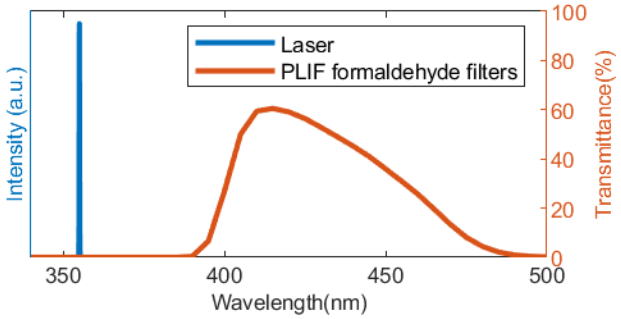

Figure 2. Laser wavelength (355 nm) used to excite formaldehyde molecules (blue) and transmittance spectrum of the set of filters used to isolate the fluorescence signal (orange).

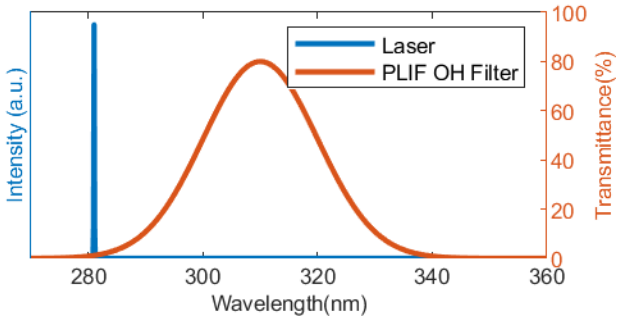

Figure 3. Laser wavelength (281.00 nm) used to excite OH radical molecules (blue) and transmittance spectrum of the filter used to isolate the fluorescence signal (orange).

A lens system was used to transform the laser spot into a sheet. It was composed by three cylindrical lenses. The first one had a focal length of -12.7 mm and a size of 15 mm x 10 mm. The second one had a focal length of 100 mm and a size of 30 mm x 45 mm. Finally, the third lens had a focal length of 500 mm and a size of 30 mm x 45 mm. The system was aligned so that the laser sheet excited the vertical symmetry plane of the flame.

In order to capture the fluorescence of the molecules, an intensified CCD camera (Andor iStar DH334T-18H-83) was used, perpendicular to the plane defined by the laser sheet (see Figure 1). The photocathode of the intensifier is a S-20 (spectral response: 180-850 nm). Light was collected by a 105-mm UV objective (Nikon f/4.5). The ICCD gating was set to 900 ns, to reduce the interference signal from other events sources such as OH* chemiluminescence or the thermal radiation of the soot. The resolution was 10.40 pixel per mm.

OH and formaldehyde fluorescence images were not acquired simultaneously. A set of UV mirrors located on a motorized table were used to alternatively align each laser beam with the lens system previously described (see Figure 1). A similar system was utilized for the camera filters. Thus, alternate measurements of OH and formaldehyde were carried out.

The frequency of the ICCD and both laser sources limit the number of images per injection that could be registered. Consequently, one frame

per injection was acquired. Measurements were performed at different instants after start of injection (ASOI).

Despite using sets of filters to avoid non-fluorescence radiation to arrive at the detector, it was not possible to remove all of it. For this reason, radiation with and without firing laser excitation was acquired. In the first case, the camera registered both induced fluorescence and other spontaneous radiation (chemiluminescence and thermal radiation of the flame). In the second case, the signal corresponded to spontaneous radiation due to chemiluminescence and thermal radiation (not radiation due to the laser). A comparison of these images can be observed in Figure 4 and Figure 5. Since this work does not intend to quantify the species concentration with this technique, no flat field correction has been made to the laser sheet.

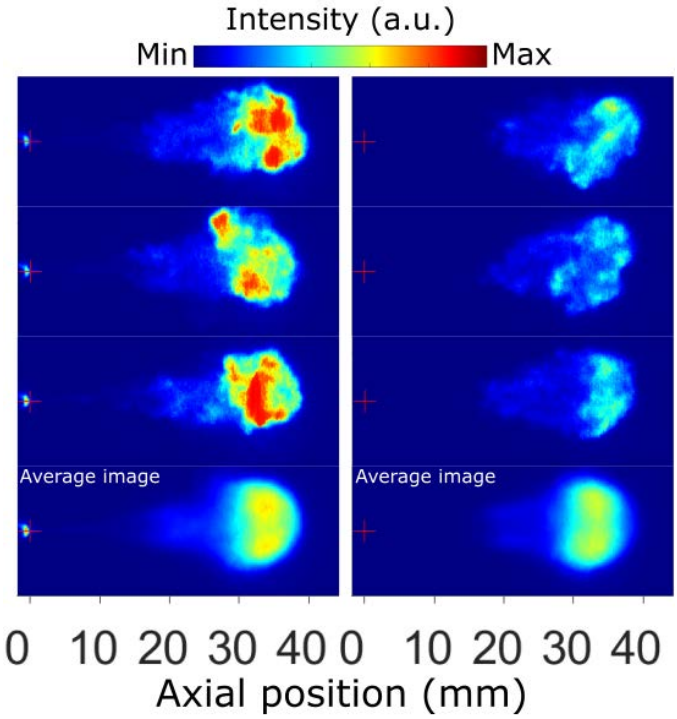

Figure 4. Images with (left) and without (right) firing the laser excitation corresponding to formaldehyde detection at 640 µs ASOI. Each image represents an unique injection event of dodecane. The last row represents the average of 50 repetitions for both columns.

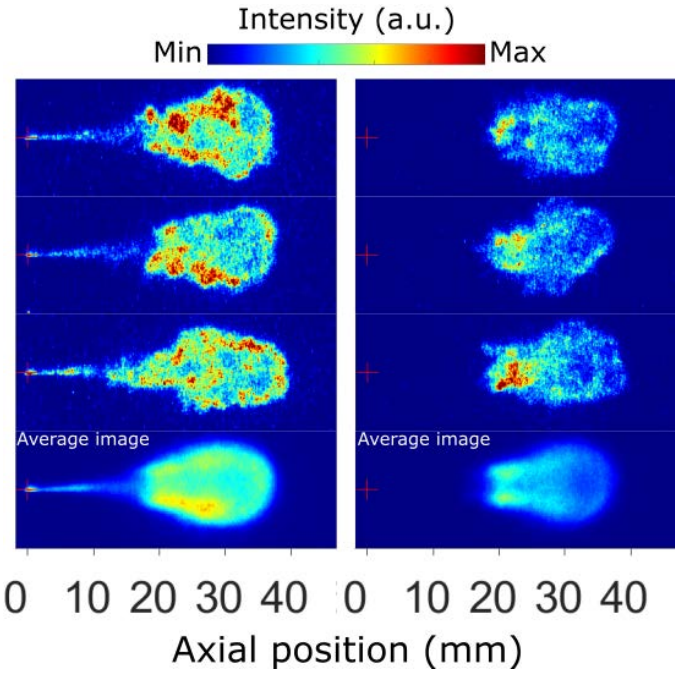

Figure 5. Images with (left) and without (right) firing the laser excitation corresponding to OH radical detection at 640 µs ASOI. Each image represents an unique injection event of dodecane. The last row represents the average of 50 repetitions for both columns.

In the previous figures, the cycle-to-cycle variability of the combustion process is clear. This instability is due to the turbulence of the flame and the stochastic behavior of the process. For this reason, 50 images with firing the laser excitation and 50 images without firing the laser excitation were registered for each instant ASOI. Then, the ensemble average of images without laser was subtracted from the one corresponding to images with laser. Therefore, the fluorescence average laser induced signal was isolated. A comparison between average signal with and without firing the laser excitation is also presented in Figure 4 and Figure 5.

Results and discussions

The different optical techniques used in this work allow to study and compare the diffusive flame structure for dodecane and oxymethylene dimethyl ether (OMEx) under Spray A conditions of the Engine Combustion Network (ECN).

In Figure 6, a sequence of OH^* chemiluminescence images at different instants ASOI for dodecane and OMEx fuels can be observed. Each frame corresponds to the average of all repetitions at each instant. High temperature reactions and therefore OH^* radiation appear earlier for the second fuel. As can be seen, at 340 µs ASOI a small spot is already visible while for dodecane the first signal appears at 420 µs ASOI. This is however not consistent with the lower cetane number of this fuel, which is related with a longer ignition delay. Nevertheless, one must keep in mind that the ignition delay can be also affected by the local oxygen availability for OMEx (thanks to its molecular structure). As mentioned previously, the OH^* chemiluminescence images for the

OME_X case were performed with an intensification level of 80% while in the dodecane it was 75%.

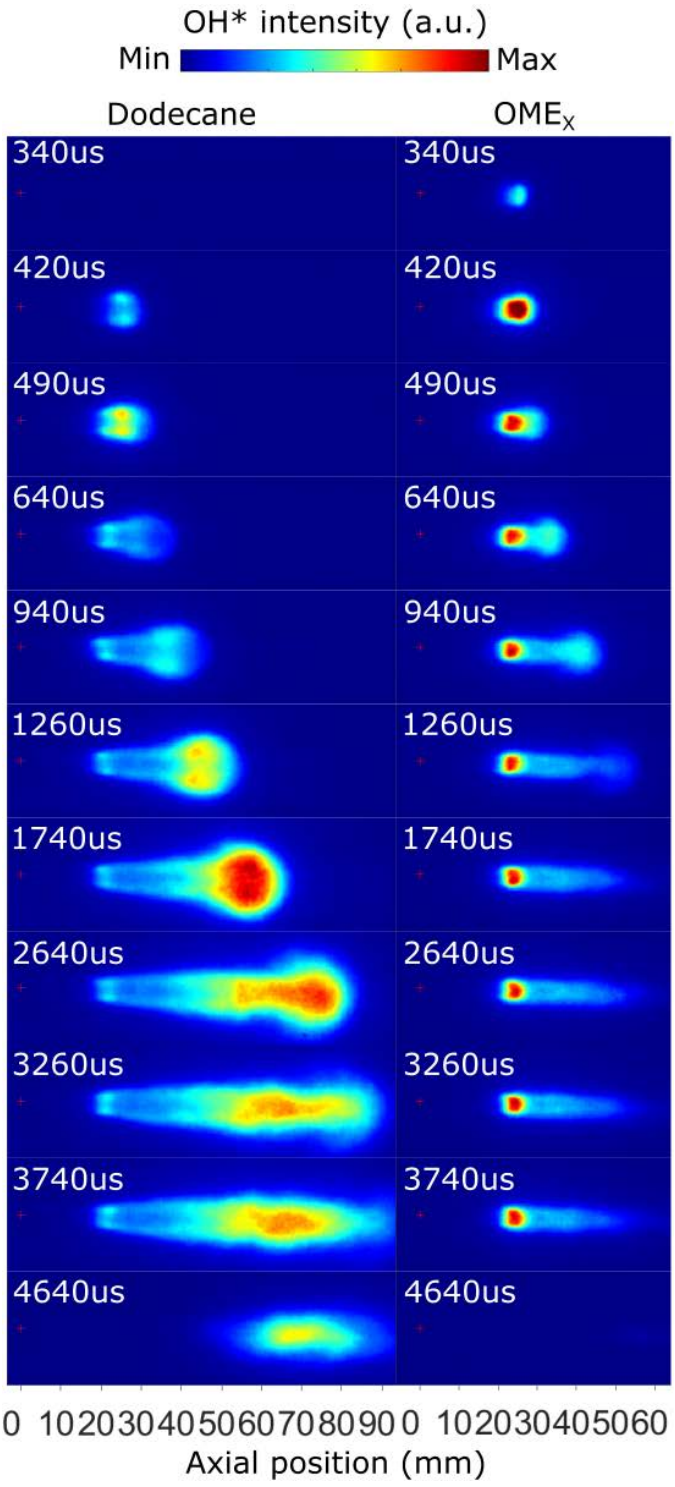

Figure 6. OH^* chemiluminescence images at different times ASOI for dodecane (left) and OME_X (right) fuels.

The analysis of OH* chemiluminescence distributions allows to obtain both flame lift-off length and penetration. In Figure 7, a comparison of both magnitudes between dodecane (red) and OME_X (green) is presented. Flame penetration, as derived from OH^* images, increases with time until reaching an approximately constant value. It can be clearly seen that the lift-off length for both fuels is quite stable from start of combustion until shortly after end of injection, with higher values for OME_X than for dodecane.

From Figure 7, a clear difference in the location and spatial structure of OH^* chemiluminescence for the two fuels can be observed. The lift-off length for dodecane is shorter (18.69 mm) than for the OME_X (20.28 mm), while the flame front length is larger for dodecane (88.28 mm) than for the OME_X (50.43 mm). OH* is expected to appear at the periphery of the spray, where high-temperature flame is located. When integrated along the line of sight, the more intense region should not appear in the center of the spray but at its periphery. This is not observed with dodecane. In this case, the brightest region in the center of the spray (downstream of ~35 mm) could be linked to soot radiation [30]. It must be noted that optical filters are not 100% effective and still a minimum percentage of high-intensity incandescence could be significant for an ICCD. Additionally, thermal radiation from soot (weak) is present even in the UV region.

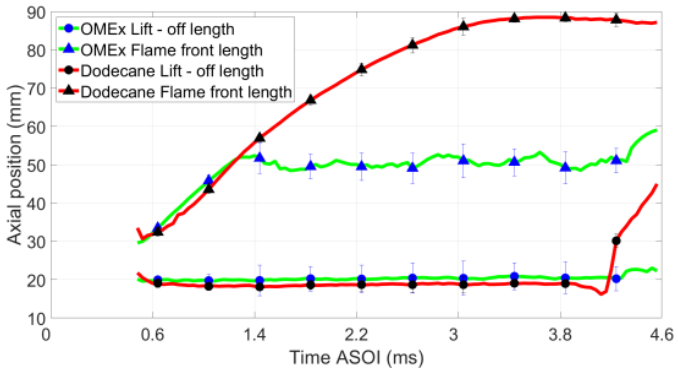

Figure 7. Comparison of the lift-off length and flame penetration front instant time ASOI for dodecane (red) and OME_X (green) fuels.

The first OH* signal detected allows to define the ignition delay, from which PLIF measurement instants where defined. In Figure 8, the fluorescence of formaldehyde and OH radical molecules for dodecane can be observed.

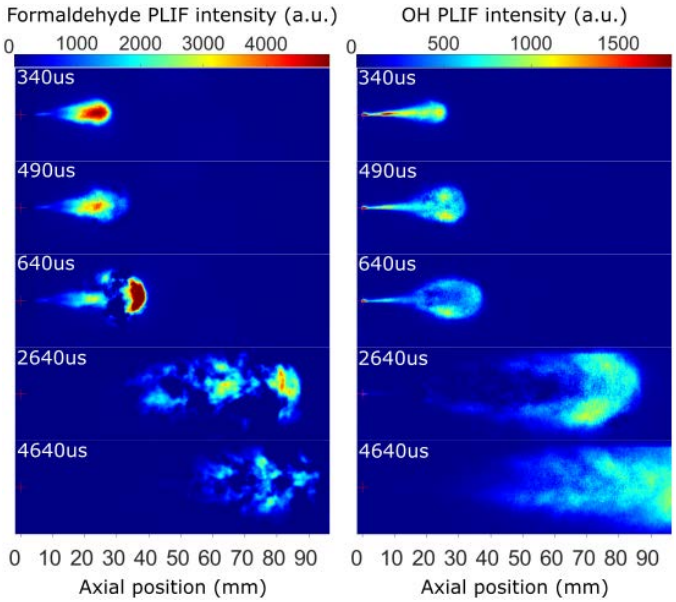

Figure 8. Fluorescence of formaldehyde (left) and OH-radical molecules (right) at different instants of time ASOI for dodecane fuel.

Starting with the initial image at 340 µs on the right, the signal does not presumably correspond with PLIF of OH. The main argument is that, as shown in Figure 6, OH* has not appeared yet at the same timing, which means that the high-temperature ignition phase has not been reached. Furthermore, the spatial location of the signal is to some extent superimposed on that of formaldehyde, which is fully inconsistent with the transition from low to high temperature ignition stages. At 490 µs, however, high temperature reactions have developed and a bigger area corresponding to OH PLIF is observed. As flame progresses, it can be seen that the highest intensity of fluorescence is located in the lateral lobes. This corresponds to the stoichiometric zone of the flame structure [31, 32].

When analyzing formaldehyde fluorescence, it is possible to see that the signal is most intense at first stages of combustion (340 µs), consistently with the fact that this molecule is an indicator of low-temperature reactions. In comparison to OH -radicals, formaldehyde disappears when high-temperature reactions occur, as confirmed by the overall lower signal at 490 µs compared to the initial image. This is particularly clear at the tip of the spray, and it confirms that the spray is running into the high temperature phase, as the peak OH* intensity at the same timing has been observed in Figure 6will be exacerbated because of laser attenuation by PAH and soot with head-on illumination. In a stabilized diesel-type flame formaldehyde can be first found upstream of the LOL and extends towards the jet center around or downstream of the LOL [33]. Consequently, with this description, the high intensity level of formaldehyde PLIF signal downstream of 25 mm from the orifice at 640 µs (Figure 8) corresponds to fluorescence of PAH induced by the laser excitation [28]. Despite this, formaldehyde signal can still be observed around the lift-off length location. Nevertheless, after 640 µs, the fluorescence signal of this molecule in the latter location is hindered due to the PAH and soot presence downstream [34]. Based on filters transmissivity, the collected radiation for these cases is mainly thermal emission from soot and fluorescence of PAH. In addition, soot at the spray tip is strongly absorptive, and does not allow radiation from the laser sheet to reach flame base, where formaldehyde presence was detected at the first stages of combustion process. In the case of the OH radical, the detected signal is mostly fluorescence thanks to the filters used. However, it must be taken into account that the soot also attenuates the laser sheet and makes it difficult to obtain fluorescence signal close to the flame lift-off. It should be noted that the signal that appears in the area of the injector is a signal due to the scattering of the laser, since that area belongs to the liquid length and therefore conditions are such that no OH radicals can be expected in this region.

For OMEx, the fluorescence of the formaldehyde and OH radical molecules at different instants ASOI can be observed in Figure 9. As it occurred for dodecane, the transition from low temperature to high temperature reactions corresponds to the appearance of OH fluorescence and the consumption of formaldehyde molecules. For this fuel, which ignites earlier than dodecane, the instants chosen clearly show the ignition process. Until 340 µs, only formaldehyde fluorescence was detected, with OH signal being quite faint. This is consistent with the fact that, at this stages, only low temperature reactions are taking place. As a consequence, OH fluorescence is visible from 540 µs ASOI, showing the high-temperature reactions. At the same time, it is observed that both intensity and area of the formaldehyde signal drastically decreases, which corresponds to a consumption of these molecules as spray ignites.

When comparing Figure 8 and Figure 9, it is possible to see that for OMEx, the two lateral lobes are more prominent than for dodecane. Additionally, the absorption problems caused by soot over fluorescence measurements are not apparent. When considering OH signal, it is possible to see that flame structure evolves uniformly. The signal corresponds very much with the OH^* chemiluminescence for the whole flame, without the clear drop in signal around the lift-off location that was observed for dodecane Even at 2640 µs, the signal intensity at the flame base is enough to clearly define the lift-off length. Besides, the whole flame structure is visible.

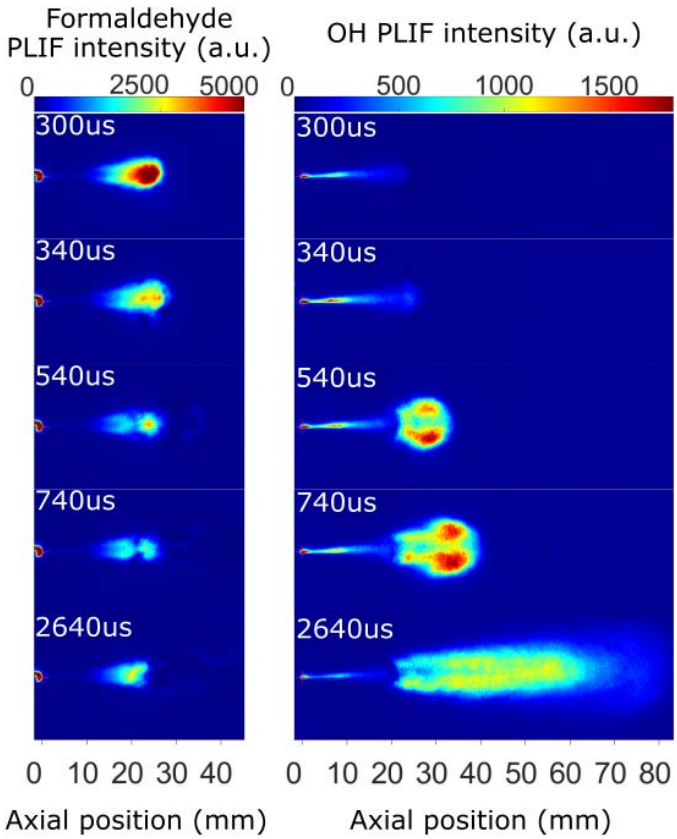

Figure 9. Fluorescence of formaldehyde (left) and OH radical molecules (right) at different instants of time ASOI for OME_X fuel.

When comparing OH* chemiluminescence (Figure 6) and OH PLIF measurements (Figure 8 and Figure 9), several differences arise. For dodecane, it can be seen how a bright spray-head moves downstream from the injector (Figure 6), presumably corresponding to soot incandescence [22, 35]. The most intense region appears at the sides of the flame at first instants, but they move towards the center and concentrate around the spray axis, close to the tip of the flame. The OH PLIF shows a similar evolution in terms of OH progression downstream the nozzle. However, the signal can be found near the flame front, both at the tip and the sides of the flame and not close to the spray axis (Figure 8). Also, it can be observed that OH* is found mainly in the flame front, especially in the LOL region where ignition take place (see Figure 6). OH, on the other hand, has longer lifetime than OH* and it can be found even downstream the stoichiometric contour of the flame. Focusing on OME_X, it can be seen in Figure 6 that the strongest OH^* chemiluminescence signal is concentrated near the injector position and remains stable throughout the combustion process. However, the OH PLIF signal (Figure 9) do not show that intense region. In contrast, the more intense spots are located at the sides of the flame (lobes) and continuously grow downstream from the injector (Figure 9) until flame length stabilization is reached.

These differences in OH detection can be related to the fact that chemiluminescence imaging and PLIF are based on different principles. The first one involves the whole flame volume, whose radiation is integrated in a two-dimension intensity map. However, the PLIF technique is exciting the symmetry plane of the flame, where the laser sheet was aligned. Thus, only OH radicals located at this plane are detected. Moreover, it must be taken into account that all OH^* states can contribute to the OH^* chemiluminescence signal, while only few rotation states contribute to the PLIF signal. Thus, the sensitivity in detecting these species is different [32]. This implies that regions with low OH concentration, will show low or null PLIF signal. Finally, it should be noted that, when taking into account the soot incandescence contribution to the dodecane flame, the relationship between OH^* and OH for both fuels is similar.

In Figure 10, formaldehyde and OH LIF signals have been superimposed. The superposition of the fluorescence images of formaldehyde (green) and OH (purple) allow to clearly see the evolution and the interaction between these two species.

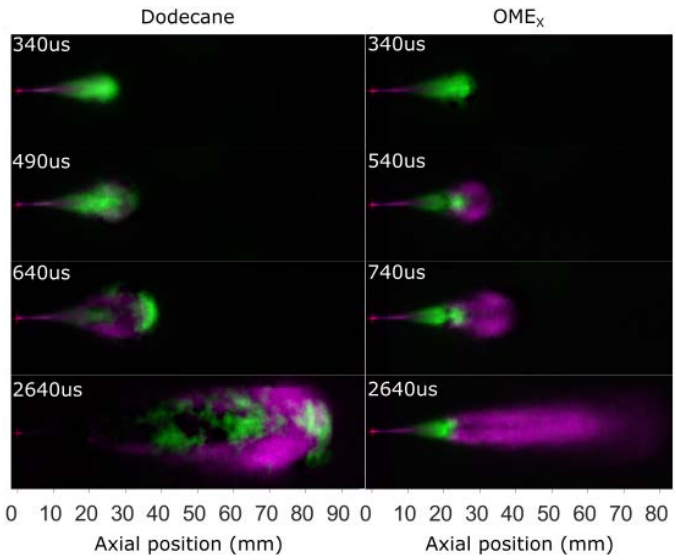

Figure 10. Superposition of the PLIF technique images (formaldehyde in green and OH in purple) for dodecane (left) and OME_X (right) fuels.

For both fuels, it can be seen how formaldehyde molecules appear for both fuels at the first instant ASOI. Later, when high-temperature reactions occur, the OH signal appears. After that, it can be observed that while OH extension increases, formaldehyde decreases and almost disappears. This indicates its consumption by the high temperature reactions. For most of the cases, both molecules appear at different regions of the flame. While formaldehyde remains closer to the nozzle and around the spray axis, OH radicals extend downstream and move toward the periphery of the flame. An interface between both species is clearly visible for OME_X. In the case of dodecane, this interface is more blurred.

In the case of the dodecane fuel, at 640 µs this structure is not observed. In this case, an intense region at the tip of the flame was measured. This area corresponds to PAH fluorescence in the fuel-rich head of the jet, evident from the upstream consumption of formaldehyde and the intensity of the signal Additionally, after 640 µs ASOI, the interaction between formaldehyde and OH radicals is not visible. The interferences caused by PAH molecules and soot do not provide reliable formaldehyde or OH detection close to the lift-off length. In fact, none of the signal that is detected downstream with the 355-nm excitation at this timing can be ascribed to formaldehyde. Cold be also PAH fluorescence.

It has been observed in different studies that fuels with high oxygen concentrations have shown significant differences in the reduction of soot formation and therefore its precursors [36]. Soot formation

depends on the equivalence ratio at the lift-off length, with higher soot formed in situation with richer equivalence ratio at the lift-off.

In the case of OME_X and dodecane, it is observed that the LOL of OME_X is slightly higher than dodecane (see Figure 7), but there is a large difference in stoichiometry, with the stoichiometric mixture fraction being 0.046 for dodecane, compared to almost 0.1 for OME_X. Hence, the equivalence ratio at the lift-off length is roughly half for OME_X compared to dodecane. This confirms the absence of soot in the former fuel, which has been confirmed in independent soot formation tests [37].

Conclusions

In this work, the OME_X diffusive flame structure has been studied. Dodecane has been used as a reference, since it has been well characterized in the literature. The study has been carried out under Spray A operating conditions, defined at the ECN. High-speed OH^* chemiluminescence and planar formaldehyde and OH LIF techniques have been employed. The main conclusions achieved are:

- OH^* chemiluminescence signal shows a different flame structure of OME_X, when compared to dodecane. The first thing that can be highlighted is that the stabilized flame structure is reached earlier, resulting in a shorter flame if compared with dodecane. The high brightest region downstream 35 mm for dodecane images is associated with thermal radiation of soot. However, this structure is not observed in the case of OME_X.

- For both fuels, formaldehyde was detected during the ignition delay period or in developed Diesel flames, as it is a tracer of low-temperature reactions zones. It is located close to the lift-off length during the whole combustion process. However, the intensity and area of the signal are reduced as the high-temperature chemical reactions consume it. This is visible for OME_X but not so clear for dodecane. The presence of soot and PAH within the flame prevent the laser sheet to reach the lift-off length region.

- For both fuels, the evolution of the OH structure is similar until the stabilized combustion is reached. However, the lobes are more prominent for OME_X than for dodecane, especially at first instants. When the quasi-steady flame has developed, OME_X shows a similar "two lateral lobes" distribution in contrast with dodecane, where measurements are difficult due to soot presence attenuation.

- For both fuels, formaldehyde remains closer to the nozzle and around the spray axis. In contrast, OH radicals appear downstream and are more concentrated towards the periphery of the flame. An interface between both species can be identified. This description is easier to observe for OME_X than for dodecane, most probably due to the previously mentioned attenuation of the laser sheet as a consequence of the presence of soot.

- Some differences have been detected between OH^* chemiluminescence and OH PLIF measured for OME_X. The first signal shows the existence of a high-intensity region at the lift-off location. However, this is not represented by the fluorescence signal, as the more intense region is located closer to the flame front.

References

1. García, A., Monsalve-Serrano, J., Villalta, D. and Lago Sari, R., "Performance of a conventional diesel aftertreatment system used in a medium-duty multi-cylinder dual-mode dual-fuel engine," Energy Convers. Manag. 184;327–337, 2019, doi: 10.1016/j.enconman.2019.01.069 .
2. Singh, A. P. and Agarwal, A. K., "Low-Temperature Combustion: An Advanced Technology for Internal Combustion Engines," In Advances in Internal Combustion Engine Research; Srivastava, D. K., Agarwal, A. K., Datta, A., Maurya, R. K., Eds.; Energy, Environment, and Sustainability; Springer: Singapore, 2018; pp 9–41. doi: 10.1007/978-981-10-7575-9_2.
3. Benajes, J., García, A., Monsalve-Serrano, J. and Boronat V., "Gaseous emissions and particle size distribution of dual-mode dual-fuel diesel-gasoline concept from low to full load," Appl. Therm. Eng. 120: 138–149, 2017, doi: 10.1016/j.applthermaleng.2017.04.005 .
4. S. Molina , A. García , J. Monsalve-Serrano , D. Estepa , Miller cycle for improved efficiency, load range and emissions in a heavy-duty engine running under reactivity controlled compression ignition combustion, Appl. Therm. Eng. 136 :161–168, 2018, doi: 10.1016/j.applthermaleng.2018.02.106 .
5. Benajes, J., García, A., Monsalve-Serrano, J. and Martínez-Boggio, S., "Potential of using OME x as substitute of diesel in the dual-fuel combustion mode to reduce the global CO 2 emissions, " Transportation Engineering 1, 100001, 2020, doi: 10.1016/j.treng.2020.01.001.
6. European Commission 2016. European Reference Scenario 2016. https://ec.europa.eu/energy/sites/ener/files/documents/20160713%20draft_publication_REF2016_v13.pdf
7. Yugo, M. and Soler, A, "A look into the role of e-fuels in the transport system in Europe (2030–2050) (literature review)," Concawe Review Volume 28, Number 1, October 2019.
8. "The potential of electricity-based fuels for based fuels for low-emission transport emission transport emission transport in the EU," LBST & dena study, 2017, https://www.vda.de/en/services/Publications/%C2%ABe-fuels%C2%BB-study---the-potential-of-electricity-based-fuels-for-low-emission-transport-in-the-eu.html
9. Bae C. and Kim, J., "Alternative fuels for internal combustion engines," Proc. Combust. Inst. 36: 3389–3413, 2017, doi: 10.1016/j.proci.2016.09.009.
10. Çelebi, Y. and Aydın, H., "An overview on the light alcohol fuels in diesel engines," Fuel. 236: 890–911, 2019, doi: 10.1016/j.fuel.2018.08.138.
11. García, A., Monsalve-Serrano, J., Martínez-Boggio, S. Rückert Roso, V. et al., "Potential of bio-ethanol in different advanced combustion modes for hybrid passenger vehicles," Renewable Energy 150: 58-77, 2020, doi: 10.1016/j.renene.2019.12.102
12. Garcia, A., Monsalve-Serrano, J., Villalta, D. and Sari, R., "Fuel sensitivity effects on dual-mode dual-fuel combustion operation for different octane numbers," Energy Conversion and Management, 201, 112137, 2019, doi: 10.1016/j.enconman.2019.112137.
13. Garcia A., Monsalve-Serrano, J. & Villalta, D. Sari, R., et al. "Potential of e-Fischer Tropsch Diesel and Oxymethyl-ether (OMEx) as fuels for the dual-mode dual-fuel concept," Applied Energy, 253, 113622, 2019, doi: 10.1016/j.apenergy.2019.113622.

14. Dworschak, P., Berger, V., Härtl, M., and Wachtmeister, G., "Neat Oxymethylene Ethers: Combustion Performance and Emissions of OME_2, OME_3, OME_4 and OME_5 in a Single-Cylinder Diesel Engine," SAE Technical Paper 2020-01-0805, 2020, https://doi.org/10.4271/2020-01-0805.
15. Iannuzzi, S.E., Barro, C., Boulouchos, K. and Burger, J., "Combustion behavior and soot formation/oxidation of oxygenated fuels in a cylindrical constant volume chamber," Fuel 167:49–59, 2016, doi: 10.1016/j.fuel.2015.11.060.
16. Härtl, M., Seidenspinner, P., Jacob, E. and Wachtmeister, G., "Oxygenate screening on a heavy-duty diesel engine and emission characteristics of highly oxygenated oxymethylene ether fuel OME1", Fuel 153:328–35, 2015, doi: 10.1016/j.fuel.2015.03.012.
17. Omari, A., Heuser, B. and Pischinger, S., "Potential of oxymethylenether-diesel blends for ultra-low emission engines," Fuel 209: 232–7, 2017, doi: 10.1016/j.fuel.2017.07.107.
18. Pastor, J.V., García, A., Micó, C. and Lewiski, F., "An optical investigation of Fischer-Tropsch diesel and Oxymethylene dimethyl ether impact on combustion process for CI engines," Applied Energy, 260, 114238, 2020, doi: 10.1016/j.apenergy.2019.114238
19. Engine Combustion Network database. https://ecn.sandia.gov/diesel-spray-combustion/
20. Payri, R., García-Oliver, J.M., Xuan, T. and Bardi, M., "A study on diesel spray tip penetration and radial expansion under reacting conditions," Applied Thermal Engineering 90:619–29, 2015, doi: 10.1016/j.applthermaleng.2015.07.042
21. Desantes, J.M., Pastor, J.V., García-Oliver, J.M. and Briceño, F.J., "An experimental analysis on the evolution of the transient tip penetration in reacting Diesel sprays," Combustion and Flame 161 (8): 2137-2150, 2014, doi: 10.1016/J.COMBUSTFLAME.2014.01.022.
22. Higgins B, Siebers D. Measurement of the flame lift-off location on DI diesel sprays using OH chemiluminescence. SAE Transactions. 2001;739–53.
23. Xuan T, Desantes JM, Pastor J V., Garcia-Oliver JM. Soot temperature characterization of Spray A flames by combined extinction and radiation methodology. Combustion and Flame. 2019;204:290–303.
24. Desantes, J.M., Pastor, J.V., Pastor, J.M. and Juliá, J.E. , Limitations on the use of the planar laser induced exciplex fluorescence technique in diesel sprays, Fuel 84 (18): 2301-2315, 2005, doi:10.1016/J.FUEL.2005.05.009.
25. Donkerbroek, A. J., A. P. van Vliet, L. M.T. Somers, N. J. Dam, and J. J. ter Meulen. 2011. "Relation between Hydroxyl and Formaldehyde in a Direct-Injection Heavy-Duty Diesel Engine." Combustion and Flame 158 (3): 564–72. doi:10.1016/j.combustflame.2010.09.024.
26. Bakker, P. C., Noud Maes, and Nico Dam. 2017. "The Potential of On- and off-Resonant Formaldehyde Imaging Combined with Bootstrapping in Diesel Sprays." Combustion and Flame 182. Elsevier Inc.: 20–27. doi:10.1016/j.combustflame.2017.03.032.
27. Dec, J. and Coy, E., "OH Radical Imaging in a DI Diesel Engine and the Structure of the Early Diffusion Flame," SAE Technical Paper 960831, 1996, https://doi.org/10.4271/960831.
28. Donkerbroek AJ, Van Vliet AP, Somers LMT, Frijters PJM, Klein-Douwel RJH, Dam NJ, et al. Time-and space-resolved quantitative LIF measurements of formaldehyde in a heavy-duty diesel engine. Combustion and Flame. 2010;157(1):155–66.
29. Kosaka H, Drewes VH, Catalfamo L, Aradi AA, Iida N, Kamimoto T. Two--dimensional imaging of formaldehyde formed during the ignition process of a diesel fuel spray. 2000.
30. Maes, N., Dam, N., Somers, B., Lucchini, T. et al., "Heavy-Duty Diesel Engine Spray Combustion Processes: Experiments and Numerical Simulations," SAE Technical Paper 2018-01-1689, 2018, https://doi.org/10.4271/2018-01-1689.
31. Pickett, Lyle M., Julien Manin, Caroline L. Genzale, Dennis L. Siebers, Mark P.B. Musculus, and Cherian A. Idicheria. 2011. "Relationship Between Diesel Fuel Spray Vapor Penetration/Dispersion and Local Fuel Mixture Fraction." SAE International Journal of Engines 4 (1): 764–99. doi:10.4271/2011-01-0686.
32. Maes N, Meijer M, Dam N, Somers B, Toda HB, Bruneaux G, et al. Characterization of Spray A flame structure for parametric variations in ECN constant-volume vessels using chemiluminescence and laser-induced fluorescence. Combustion and Flame. 2016;174:138–51.
33. Idicheria, C. and Pickett, L., "Formaldehyde Visualization Near Lift-off Location in a Diesel Jet," SAE Technical Paper 2006-01-3434, 2006, https://doi.org/10.4271/2006-01-3434.
34. Bruneaux, G. 2008. "Combustion Structure of Free and Wall-Impinging Diesel Jets by Simultaneous Laser-Induced Fluorescence of Formaldehyde, Poly-Aromatic Hydrocarbons, and Hydroxides." International Journal of Engine Research 9 (3): 249–65. doi:10.1243/14680874JER00108.
35. Dec, J. and Espey, C., "Chemiluminescence Imaging of Autoignition in a DI Diesel Engine," SAE Technical Paper 982685, 1998, https://doi.org/10.4271/982685.
36. Mueller, C., Pitz, W., Pickett, L., Martin, G. et al., "Effects of Oxygenates on Soot Processes in DI Diesel Engines: Experiments and Numerical Simulations," SAE Technical Paper 2003-01-1791, 2003, https://doi.org/10.4271/2003-01-1791.
37. José V. Pastor, et al., "Experimental Study of the Effect of Alkanes and Oxymethylene Ethers Fuels on Main Spray and Combustion Characteristics under Diesel-like Conditions by Means of Optical Techniques," (under preparation).

Acknowledgments

The research leading to these results has received funding from the European Union's Horizon 2020 Programme, grant agreement n° 828947, and from the Mexican Department of Energy, CONACYT-SENER Hidrocarburos grant agreement n° B-S-69926.

Definitions/Abbreviations

OME_X	Oxymethylene dimethyl ether
ECN	Engine Combustion Network
PLIF	Planar Laser-Induced Fluorescence
UV	Ultraviolet
ICCD	Intensified charge-coupled device
ASOI	After start of injection
OH^*	Excited state of hydroxyl radical

RCCI	Reactivity controlled compression ignition
GHG	Greenhouse gas
CPF	Constant-pressure flow
PAH	Polycyclic aromatic hydrocarbons
LTC	Low temperature combustion
EGR	Exhaust gas recirculation
LIF	Laser induced fluorescence
PLIF	Planar laser-induced fluorescence
FWHM	Full width at half maximum
CMOS	Complementary metal oxide semiconductor
LOL	Lift-off length
FFL	Flame front length
FL	Focal-length
e – fuels	Synthetic fuels
CL	Chemiluminescence